Geophysical Journal International

Geophys. J. Int. (2010) **180,** 23–33 doi: 10.1111/j.1365-246X.2009.04404.x

Long wavelength convection, Poiseuille–Couette flow in the low-viscosity asthenosphere and the strength of plate margins

Tobias Höink and Adrian Lenardic

Department of Earth Science, Rice University, Houston, TX, USA. E-mail: tobias.hoeink@rice.edu

Accepted 2009 September 29. Received 2009 September 29; in original form 2009 August 10

SUMMARY

Mixed heated 3-D mantle convection simulations with a low-viscosity asthenosphere reveal relatively short and long wavelength regimes with different scalings in terms of surface velocity and surface heat flux and show that mantle flow in the lithosphere–asthenosphere region is a Poiseuille–Couette flow. The Poiseuille/Couette velocity magnitude ratio, D/U, allows us to characterize solid-state flow in the asthenosphere and to predict the regime transition. The transition from dominantly pressure-driven Poiseuille flow at shorter wavelengths to dominantly shear-driven Couette flow at long wavelengths depends on the relative strength of lithosphere and asthenosphere and is associated with a switch in the dominant resistance to convective motion. In the Poiseuille regime significant resistance is provided by plate-bending, whereas in the Couette regime most resistance is due to vertical shear in the bulk mantle. The Couette case corresponds to classical scaling ideas for mantle convection whereas the Poiseuille case, with asthenospheric velocities exceeding surface velocities, is an example of a sluggish lid mode of mantle convection that has more recently been invoked for thermal history models of the Earth. Our simulations show that both modes can exist for the same level of convective vigour (i.e. Rayleigh number) but at different convective wavelengths. Additional simulations with temperature- and yield-stress dependent viscosity show consistent behaviour and suggest an association of the regime crossover with the relative strength of plate margins. Our simulations establish a connection between the strength of plate margins, solid-state flow in the asthenosphere and the wavelength of mantle convection. This connection suggests that plate tectonics in the sluggish lid mode is wavelength dependent and potentially more robust than previously envisioned.

Key words: Planetary tectonics; Dynamics of lithosphere and mantle; Dynamics: convection currents, and mantle plumes; Rheology: crust and lithosphere; Rheology: mantle.

1 INTRODUCTION

The role the asthenosphere plays in the Earth's mantle convection system and, by association, plate tectonics is a fundamental geodynamic question. Seismological evidence has long suggested that a sublithospheric channel of low velocity exists beneath the oceanic lithosphere (e.g. Gutenberg 1959). Evidence that this region is mechanically weak (e.g. Anderson & Sammis 1970) fuelled early considerations of its role in facilitating plate tectonics based on the idea that a low-viscosity region would 'lubricate' the base of plates. Geodynamic studies of the geoid and post-glacial rebound have confirmed the picture of a low-viscosity region within the upper mantle and are consistent with the notion that the region can be confined to the uppermost, sublithospheric mantle (Hager & Richards 1989; Thoraval & Richards 1997; Paulson & Richards 2009). The low viscosity of the asthenosphere may be due to partial melt (e.g. Anderson & Sammis 1970; Anderson & Spetzler 1970) and/or the weakening effects of water (e.g. Karato & Jung 1998). The combination of water and melting can also work in another way to influence the viscosity structure of the oceanic lithosphere–asthenosphere system: water extraction at mid-ocean ridges during mantle melting can result in a viscosity jump of 2–3 orders of magnitude from the asthenosphere to the newly formed, and dehydrated, lithosphere (Hirth & Kohlstedt 1996). Although water and melt may play a role, it should be noted that the cause(s) of a seismic low-velocity zone and a low-viscosity asthenosphere remain debated (Stixrude & Lithgow-Bertelloni 2005; Marone & Romanowicz 2007).

Although the origin of a low-viscosity asthenosphere remains an open question, the long-standing evidence of its existence together with constraints on its thickness and relative viscosity allow for the consideration of its geodynamic effects. Advances in the numerical simulation of mantle convection provided a platform for such considerations and fuelled a second wave of interest in the dynamic role of the asthenosphere in the solid Earth system. Although some numerical studies have suggested that a moderately strong lithosphere can lead to long wavelength convection (e.g. Harder 2000; McNamara & Zhong 2005; Zhong *et al.* 2007), a number of numerical simulation studies have highlighted the ability

of a low-viscosity channel, an asthenosphere analog, to promote long wavelength thermal convection (e.g. Bunge *et al.* 1996, 1997; Tackley 1996; Richards *et al.* 2001; Zhong & Zuber 2001; Roberts & Zhong 2006; Zhong *et al.* 2007). This observation from numerical studies received particular attention given seismological evidence that convection in the Earth's mantle is dominated by long wavelength structure (e.g. Su & Dziewonski 1992). The observation is also potentially pertinent for understanding the dynamic link between mantle convection and plate tectonics. Plate tectonics is the primary surface manifestation of mantle convection and the lateral extent of plates relative to the depth of the mantle suggests a long wavelength mode of convection.

The numerical simulations noted earlier were valuable in focusing attention to the importance of the asthenosphere in the Earth's mantle convection system. They did not, however, provide a physical understanding of how the asthenosphere allows for long wavelength flow within the mantle. In an effort to move in this direction, Busse *et al.* (2006) and Lenardic *et al.* (2006) used modifications of established boundary layer theory to formulate a physical analysis of the effects of low-viscosity channels on thermal convection. The principal conclusion was that low-viscosity layers within a convecting mantle can lead to a flow channelization that lowers the lateral dissipation associated with convection cells. This allows larger aspect ratio cells to form as the ratio of channel-to-bulk mantle viscosity decreases. In the absence of flow channelization, the horizontal length scale of convection is limited by the rapid increase in horizontal shear dissipation that occurs as convection cells grow longer. The theoretical analysis assumed Couette flow within the low-viscosity channels, that is, the velocity within the channel decreased linearly from its top to its base. Confinement of lateral flow within a thin channel increased the strain rate in the channel but its low viscosity outweighed this effect in determining horizontal shear dissipation. 2-D numerical simulations confirmed the theory predictions at low to medium levels of convective vigour, that is mild Rayleigh numbers. However, at higher Rayleigh numbers small-scale boundary layer instabilities formed and disrupted the channelized Couette flow. This increased lateral dissipation negating the 'advantage' of longer convection cells afforded by a low-viscosity channel. Lenardic *et al.* (2006) hypothesized that if the low-viscosity channel resided beneath a higher viscosity layer, a lithosphere analog, then the short wavelength instabilities would be inhibited, and the effect of the asthenosphere on cell length might be restored. Added numerical simulations with a low-viscosity channel submerged below a higher viscosity layer showed that small-scale instabilities were inhibited and longer wavelength convection cells could be stabilized at relatively high Rayleigh numbers.

The analysis of Busse *et al.* (2006) and Lenardic *et al.* (2006) was limited to bottom or internally heated convection and numerical testing was done with 2-D simulations. Höink & Lenardic (2008) extended the testing to 3-D simulations with mixed bottom and internal heating. Several of the results were consistent with the assumptions and predictions of Busse *et al.* (2006) and Lenardic *et al.* (2006) (lateral flow was channelized to the low-viscosity asthenosphere, longer wavelength cells were associated with greater heat loss and internal cooling indicating that lateral dissipation increased relatively slowly with cell extent). However, the simulations also highlighted some deficiencies in terms of understanding the combined role of a high-viscosity plate analog and a low-viscosity asthenosphere. The hypothesis of Lenardic *et al.* (2006) was that the high-viscosity plate would inhibit small-scale boundary layer instabilities but that in all other regards the main assumptions of the physical analysis would carry over. Specifically, for a dominantly internally heated mantle it was assumed that the principal viscous resistances to convective motion were associated with the horizontal shear stress imposed on the asthenosphere by the lateral motion of plates and the vertical shear stress imposed on the bulk mantle by descending slabs. To quantify these shear terms it was further assumed that the velocity gradients within the asthenosphere and mantle could be approximated as linear with peak horizontal and vertical velocities being associated with the near-surface plate and the descending cold slab, respectively. The simulations of Höink & Lenardic (2008) showed that the near-surface plate analog moved slower than the peak velocity in the asthenosphere and that flow in the asthenosphere, although still channelized, was not of Couette type. Collectively, this indicated that the plate analog was providing a resistance to motion that was not accounted for in the analysis of Busse *et al.* (2006) and Lenardic *et al.* (2006). As the wavelength of convection, that is cell aspect ratio, was increased the plate velocity increased and the flow in the asthenosphere approached the Couette end-member. It was speculated that the system was moving towards a very long wavelength regime in which the relative plate resistance was no longer playing a dominant role. The modelling domain size of the simulations allowed for a maximum cell aspect ratio of eight and the long wavelength regime was not reached.

In this paper, we extend the simulations of Höink & Lenardic (2008) to larger modelling domains. We find that there are two scaling regimes, one at relatively small convective wavelengths and the other at large wavelengths. Flow in the lithosphere–asthenosphere region is a Poiseuille–Couette flow with the Poiseuille component dominating at small wavelengths and the Couette component dominating at large wavelengths. The Poiseuille flow regime corresponds to a sluggish lid mode of convection, in which velocities in the asthenosphere exceed surface velocities and the resistance to motion from plate margins (plate-bending) and viscous dissipation in the interior are comparable. The Couette flow regime corresponds to the classical active lid idea of mantle convection with sublithospheric shear flow and resistance to motion solely provided by internal viscous dissipation. We find that the transition between these two regimes is characterized by distinct breaks in the scaling behaviour of surface heat flux and velocity and can be predicted by the Poiseuille/Couette velocity magnitude ratio. Our layered viscosity simulations motivate viscoplastic simulations which provide an improved analog for generating plate-like behaviour in convection models. The combined sets of simulations indicate that the two regimes mapped are wavelength dependent and associated with relatively strong or relatively weak plate boundaries interacting with a low-viscosity asthenosphere. We end by discussing the implications for convection in the Earth's mantle as well as noting future modelling work that is motivated by our results.

2 METHODS

We have performed mantle convection simulations with a submerged thin low-viscosity channel, which represents the asthenosphere in Earth's mantle. The entire system is cooled from above and heated from below and from within. We used three Cartesian geometries shown in Fig. 1: (1) full 3-D of spatial extent Γ:Γ:1, where Γ is the aspect ratio (ratio of box height-to-box width), (2) small 3-D (Γ:1:1) and (3) 2-D (Γ:1). We have chosen to use the latter two geometries once we realized that the flow in full 3-D developed long wavelength statistically steady states that could be described in two dimensions (see Figs 1d and f). The latter two geometries allow us to investigate the parameter space more efficiently. In addition,

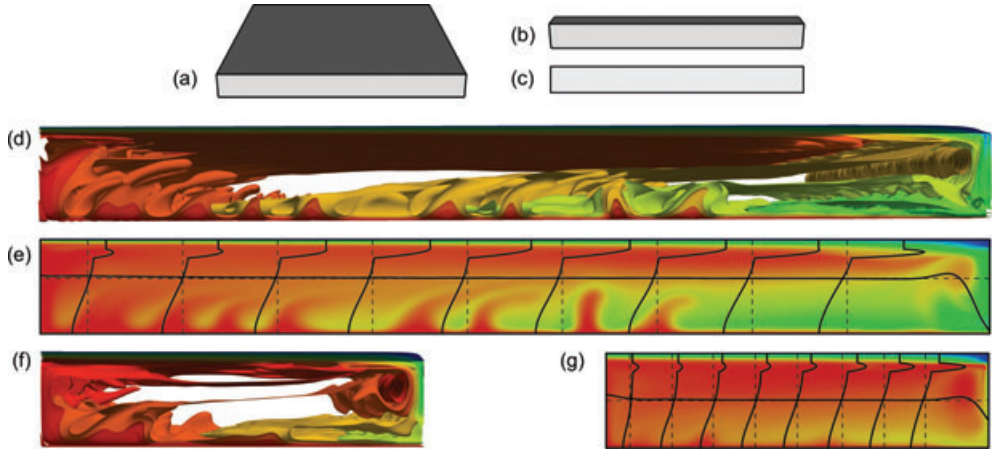

Figure 1. Geometries used in this work and typical flow field in statistically steady state. (a) Full 3-D with aspect ratio Γ:Γ:1, (b) small 3-D with aspect ratio Γ:1:1 and (c) 2-D with aspect ratio Γ:1. Front views of temperature isosurfaces from full 3-D simulation with aspect ratio 10:10:1 (d) and 4:4:1 (f). The flow is largely organized in 2-D. (e, g) Velocity profiles drawn on top of temperature field front view from same simulation as in (d, f).

we are able to report to which degree the resource-intensive full 3-D simulations can be replaced by smaller small 3-D or even 2-D simulations.

The Boussinesq equations governing thermal convection in an incompressible, infinite-Prandtl number fluid are solved with CitcomCU (Moresi & Gurnis 1995; Zhong 2006), where we used the finite element full multigrid solver for 3-D simulations and the conjugated gradient solver for 2-D simulations. All boundaries are free slip. We have used grid refinement in the top of the domain that is associated with the lithosphere and asthenosphere, and in some cases also at the basal boundary.

We prescribe a vertically layered viscosity structure simulating the strong compositional boundary layer above a weaker asthenosphere (Hirth & Kohlstedt 1996). Unless otherwise noted, we have used the following parameters (with default values in parenthesis): Rayleigh number (Ra $= 10^6$), Internal heating rate ($Q = 10$), system depth ($H = 1$), low-viscosity channel thickness ($d_A = 0.1$), surface layer thickness ($d_L = 0.1$), low-viscosity channel viscosity ($\mu_A = 0.01$), surface layer viscosity ($\mu_L = 10$), convective core viscosity ($\mu_c = 1$). We systematically varied the aspect ratio Γ and the domain width W, and report on domain-filling convection cells from full 3-D simulations ($\Gamma = 1, 2, 3, 4, 5, 8, 10$; $W = \Gamma$), small 3-D simulations ($\Gamma = 2, 4, 8, 10, 16$; $W = 1$), and 2-D simulations ($\Gamma = 8, 10, 16, 32$; $W = 0$).

The first six simulations are congruent with previous work (Höink & Lenardic 2008), which found that surface heat flux increased, and internal temperature decreased with aspect ratio up to $\Gamma = 8$. These trends are not expected to continue indefinitely. We extended our simulations to larger aspect ratios to find the transition and with the hope to characterize the system beyond this transition.

3 SIMULATION RESULTS

3.1 Diagnostics

Fig. 2 summarizes how the diagnostic output quantities surface velocity, maximum velocity in the low-viscosity channel, heat flux and internal temperature change with aspect ratio. A transition between two regimes, at an aspect ratio near 10, is indicated by different scalings between surface velocity and aspect ratio (Fig. 2a), where the power-law exponent changes significantly. Surface heat flux shows a less pronounced break in scaling behaviour also around aspect ratio 10 (Fig. 2c) and shows a maximum, consistent with a minimum of internal temperature (Fig. 2d), at aspect ratio 16.

It is interesting to note here—and we will discuss this point later in more detail—that the maximum velocity in the low-viscosity channel exceeds the surface velocity for small aspect ratios.

The internal heating ratio is another diagnostic parameter and can be computed after the simulations reach statistically steady state. The internal heating ratios from the simulations presented here vary between about 96 per cent and 87 per cent depending on the aspect ratio. We also find a consistent correlation between internal heating ratio and internal temperature: cases with higher internal heating ratios show a higher internal temperature. We stress here that the internal temperature changes as a function of aspect ratio. This is particularly interesting because the internal temperature in simulations relates to the mantle potential temperature, which is an important quantity with respect to melting, crust formation and core heat flux. The aspect ratio of convection cells in Earth's mantle therefore has a first-order control on Earth's ability to cool and on its thermochemical history.

3.2 Geometries

In comparing different geometries, we find that statistically steady states of full 3-D simulations are reproduced very well by small 3-D simulations. This allows one to reduce computational costs significantly, because the domain for small 3-D computations only scales linearly with aspect ratio, compared to a square dependence for full 3-D simulations. We find that 2-D simulations reproduce the trends of diagnostic quantities of the full 3-D simulations reasonably well (Fig. 2). However, differences are observed in quantities associated with heat transport characteristics: 2-D simulations consistently underpredict velocities and surface heat flux, and overpredict internal temperatures. Although the upwellings in 2-D represent sheets, they are plumes in 3-D. The small 3-D geometry allows the sheets to breakup sufficiently into plumes with a characteristic width smaller than the width of the box. Therefore, the small 3-D geometry recovers the results of the full 3-D geometry. With increasing internal temperatures, the convective system moves more towards the purely

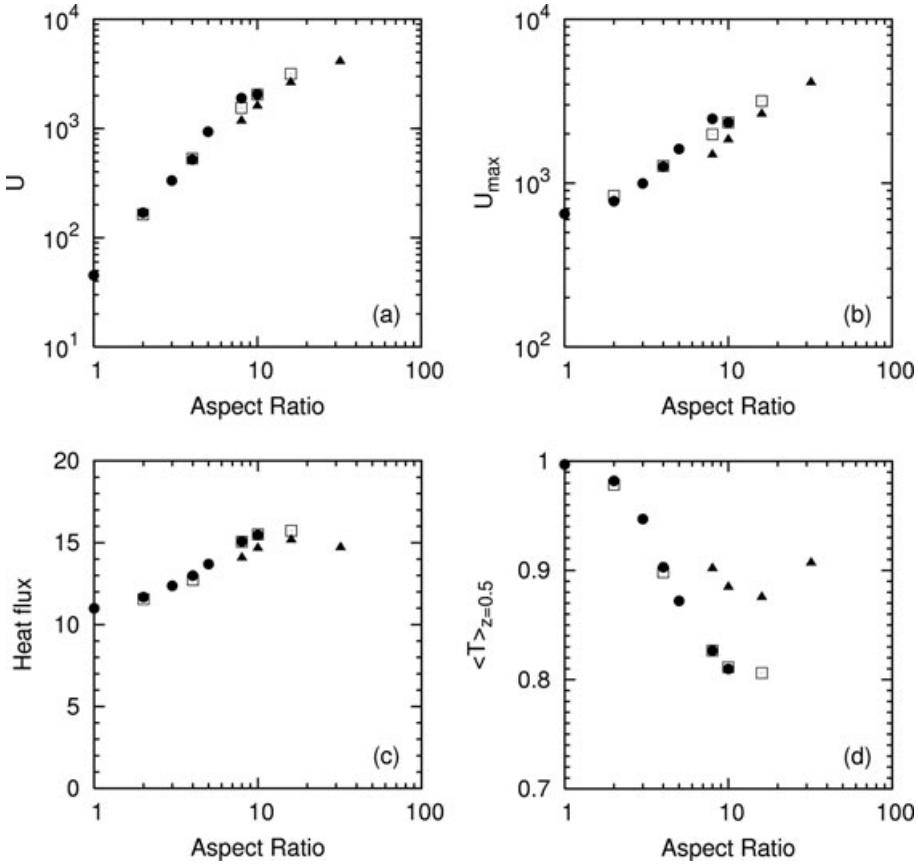

Figure 2. Results from our simulations. (a) Surface velocity, (b) maximum velocity, (c) surface heat flux and (d) internal temperature (horizontally averaged temperature at mid-depth). Symbols indicate different geometries: full 3-D (solid circles), small 3-D (squares) and 2-D (triangles). Results from both 3-D geometries agree very well, whereas 2-D simulations do not capture the heat transport characteristics.

internally heated end-member which is associated with lower velocities. This is consistent with the observed lower velocities in the 2-D simulations.

4 POISEUILLE–COUETTE FLOW IN THE ASTHENOSPHERE

4.1 Poiseuille–Couette flow

The laterally averaged horizontal velocity profiles from our 3-D geometry simulations are shown in Fig. 3(a), where we have zoomed into the region of the low-viscosity channel, that is the asthenosphere in Earth's terms. Close inspection of these profiles shows that (1) flow velocities in the low-viscosity channel exceed surface velocities considerably for smaller aspect ratios and (2) for larger aspect ratios the top of the low-viscosity channel, that is the lithosphere in Earth's terms, moves at comparable velocity compared with the velocity in the low-viscosity channel. We suspect that lateral flow in the low-viscosity channel shows a superposition of a linear velocity profile, which has the appearance of a Couette flow, that is driven by a moving horizontal plate, and a Poiseuille flow. To test this hypothesis, we assume that the velocity in the low-viscosity channel is a pressure-driven flow bounded by two rigid surfaces at top and bottom, both of which might be moving. The resulting velocity profile will then have the general form of a unidirectional Poiseuille–Couette flow

$$U_{\mathrm{A}}(z') = -D\left(\frac{z'^2}{{d_{\mathrm{A}}}^2} - \frac{z'}{d_{\mathrm{A}}}\right) + (U - U_{\mathrm{c}})\frac{z'}{d_{\mathrm{A}}} + U_{\mathrm{c}}, \tag{1}$$

where U_{A} is the low-viscosity channel (asthenosphere) velocity that depends on the vertical coordinate $z' \in [0, d_{\mathrm{A}}]$. The channel thickness is given by d_{A}, and U and U_{c} are, respectively, the top (lithosphere) velocity and bottom (core of convection cell) velocity. The magnitude of the Poiseuille flow component is given by

$$D = \frac{{d_{\mathrm{A}}}^2}{2\mu_{\mathrm{A}}}\frac{\mathrm{d}p}{\mathrm{d}x}, \tag{2}$$

where $\frac{\mathrm{d}p}{\mathrm{d}x}$ is the horizontal pressure gradient and μ_{A} is the channel viscosity. The magnitude of the Couette flow component is given by $(U - U_{\mathrm{c}})$.

We compute synthetic velocity profiles to be compared against the velocity profiles from the simulations. For each of the profiles shown in Fig. 3(a), we measured the velocity at the top (U) and bottom (U_{c}) of the low-viscosity channel. We then subtract the Couette contribution from the velocity profile and find the maximum ($U_{\mathrm{A_{max}}}$) of the remaining parabolic profile. From $U_{\mathrm{A_{max}}}$, we compute the Poiseuille magnitude as $D = 4U_{\mathrm{A_{max}}}$, which in turn allows us to compute $U_{\mathrm{A}}(z')$ using eq. (1). The results are shown in Fig. 3(b). We find an excellent agreement between the simulation results and the synthetic velocity profiles, especially for larger aspect ratios, and will consider the low-viscosity flow to be of Poiseuille–Couette type for our analysis.

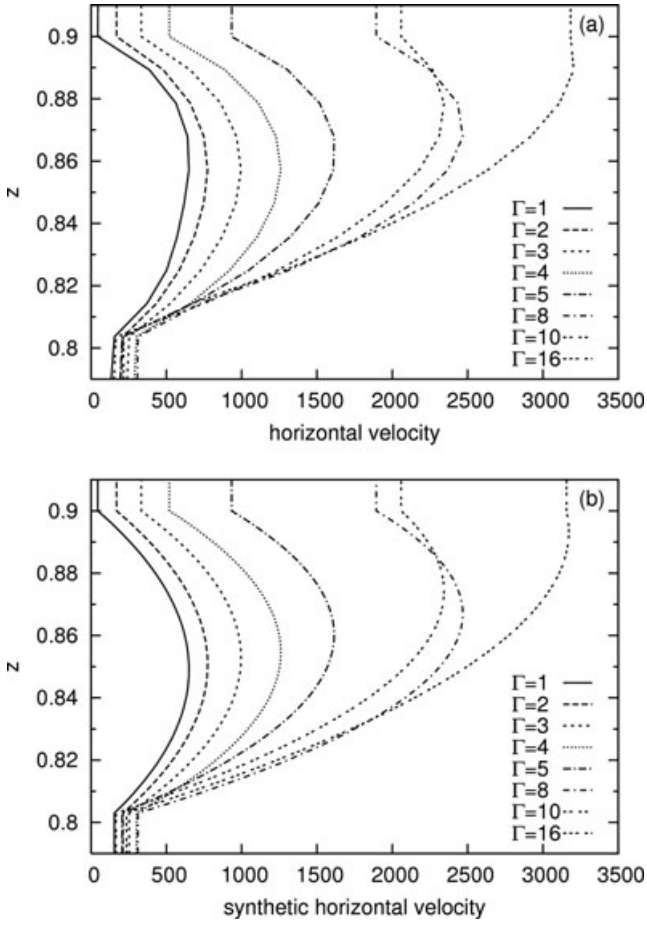

Figure 3. Comparison of measured and synthetic velocity profiles in low-viscosity channel. (a) Laterally averaged horizontal velocity profiles from 3-D numerical simulations with different aspect ratio Γ (full 3-D for $\Gamma \leq 10$, small 3-D for $\Gamma = 16$). (b) Synthetic velocity profiles of Poiseuille–Couette flow for corresponding aspect ratios computed with eq. (1).

4.2 Limit $U_c = 0$

It was noted earlier (Lenardic *et al.* 2006; Höink & Lenardic 2008) that there is no significant horizontal transport in the subasthenospheric core of the convection cell when a low-viscosity channel is present. It is therefore not surprising that U_c is small compared to U and U_{max} for large aspect ratios (see Fig. 3). Because we are interested in large aspect ratios, we will now consider the limit $U_c = 0$, which reduces eq. (1) to

$$U_A(z') = -D\left(\frac{z'^2}{{d_A}^2} - \frac{z'}{d_A}\right) + U\frac{z'}{d_A}. \quad (3)$$

In this limit, the relative magnitude of Poiseuille flow to Couette flow is given by D/U, which will emerge to be a fundamental and universal variable for this system. For $D/U \gg 1$, the flow inside the low-viscosity channel is purely pressure-driven, whereas it is a simple shear flow for $D/U \ll 1$. At $D/U \approx 1$, the flow transitions from pressure-driven to shear flow. In this transition, the maximum velocity moves from the inside of the low-viscosity channel to its surface. The maximum velocity for this system, U_{max}, normalized by the surface velocity, U, should then follow:

$$\frac{U_{max}}{U} = \frac{1}{4}\frac{D}{U} + 1. \quad (4)$$

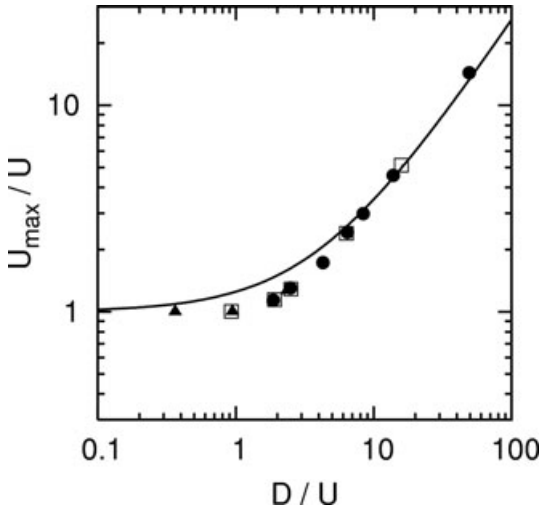

Figure 4. Maximum velocity normalized by surface velocity versus D/U from our simulations (symbols) compared to prediction from Poiseuille flow to Couette flow in the absence of subasthenospheric flow (solid line).

Fig. 4 compares the prediction from eq. (4) with our simulations and shows good agreement.

4.3 Velocity profiles downstream

Although the horizontally averaged lateral velocity profile allows us to distinguish between a predominantly pressure-driven asthenosphere and a predominantly surface-driven asthenosphere, it is also interesting to see the lateral velocity profile as a function of position. For a small aspect ratio case ($\Gamma = 4$) and a large aspect ratio case ($\Gamma = 16$), we show velocity components D and U as a function of downstream location x in Figs 5(a) and (c), and velocity profiles in the low-viscosity channel at different positions in Figs 5(b) and (d). The large aspect ratio case shows a wide zone ($3 \lesssim x \lesssim 13.6$) in which the pressure-driven flow component (D) becomes smaller than the shear flow component (U), that is $D/U < 1$ (Fig. 5c). In this region, the flow is predominantly of Couette type. This is not the case for the smaller aspect ratio case (Fig. 5a). For both cases, the flow is of Poiseuille type close to the side walls, because the horizontal surface velocity decreases to zero in regions associated with upwelling and subduction. The very large pressure at the subduction side occurs because of a bottleneck-effect between thickened lithosphere and hot rolls, which are patches of hot material that is transported inside the asthenosphere and is too buoyant to subduct. We deduce that the lateral pressure difference that, in part, drives the asthenosphere can be attributed principally to subduction processes rather than to the influx of plumes. This conclusion is also supported by Figs 1(e) and (g), which shows the strongest pressure near the subduction side.

It has previously been proposed that flow in the asthenosphere may have a Poiseuille component with a velocity exceeding plate velocity (Morgan & Smith 1992; Morgan *et al.* 1995), and this concept has been used to predict asthenosphere flow using a specific asthenosphere flow modelling technique (Yamamoto *et al.* 2007). To the best of our knowledge, however, our simulations are the first numerical confirmation of the dynamic plausibility of this flow mode. A significant difference between our current work and the hypothesis of Morgan *et al.* (1995), who considered a plume-fed buoyant asthenosphere, is that, as we have argued earlier, Poiseuille–Couette

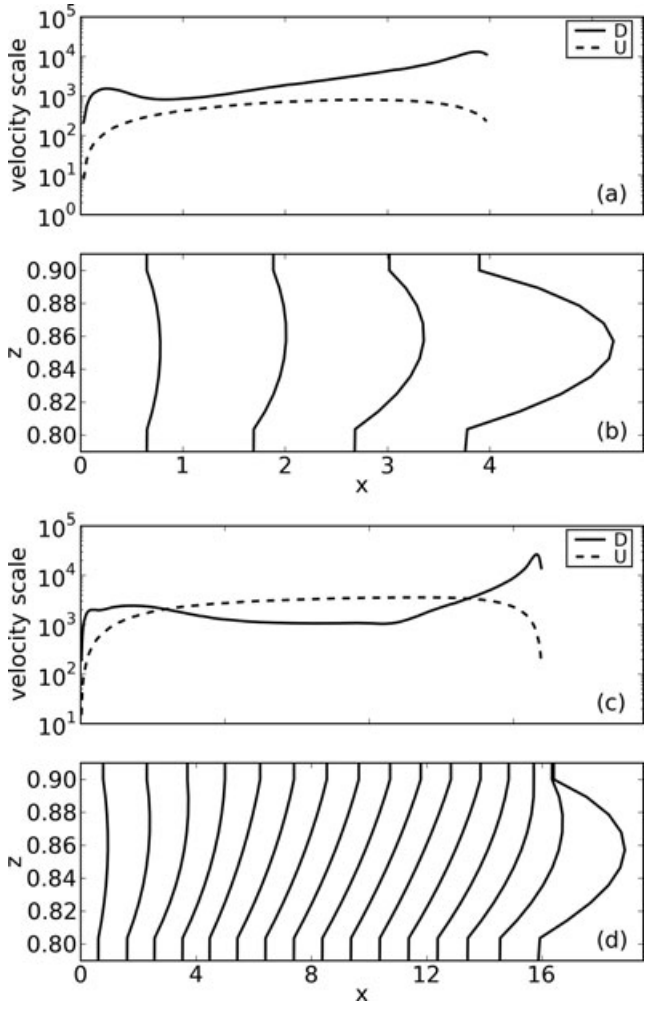

Figure 5. Flow characteristics for small aspect ratio case ($\Gamma = 4$, top panel) and large aspect ratio case ($\Gamma = 16$, bottom panel). (a, c) Poiseuille magnitude D and surface velocity U versus distance x. (b, d) Horizontal velocity profiles in the low-viscosity channel along the flow direction after averaging over intervals $\Delta x = 1$. Velocity is scaled by 2500 (b) and 1500 (d) and a zero velocity would plot in the interval centre.

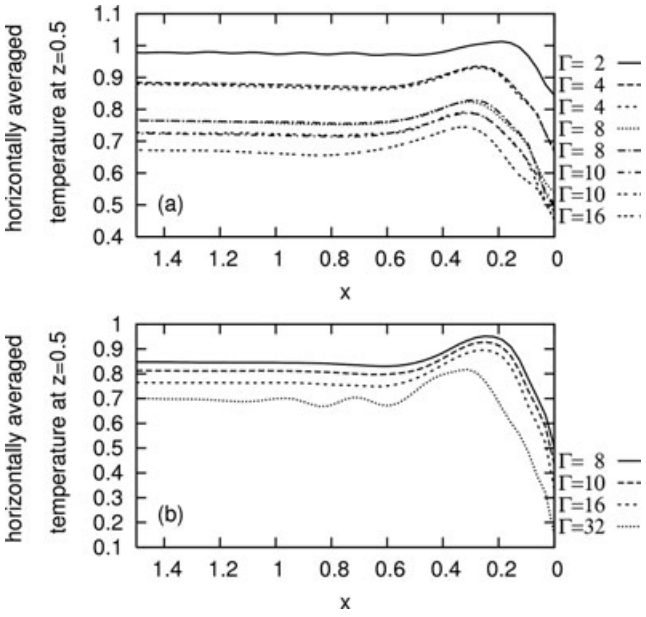

Figure 6. The horizontally averaged temperature profiles at mid-depth ($z = 0.5$) for different aspect ratios allow us to estimate the available buoyancy force due to subduction. (a) 3-D simulations and (b) 2-D simulations.

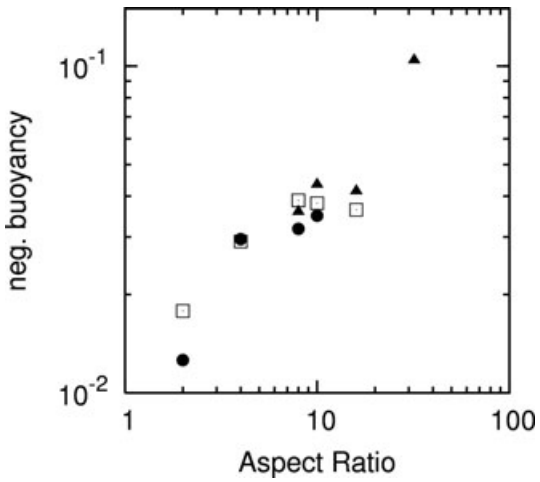

Figure 7. The available buoyancy due to the sinking slab increases with aspect ratio. The transition between Poiseuille flow and Couette flow in the asthenosphere occurs when the available buoyancy exceeds the bending resistance in the plate.

flow in our simulation is subduction driven. This implies that it can be maintained in a dominantly internally heated mantle and does not rely on the existence of plumes. It is noteworthy that 'pressure-driven' does not necessarily mean 'plume-pushed' and that a significant pressure gradient is generated by 'slab-suction'.

4.4 Buoyancy force

Fig. 2(d) shows that the interior is cooled more at longer aspect ratios. Consistent with this finding are horizontally averaged temperature profiles at mid-depth (Fig. 6). The temperature difference between interior and slab together with the slab thickness from these profiles allow us to compute the available negative buoyancy force from the sinking slab. The negative buoyancy due to slab descent, computed as the product of slab width at mid-depth and temperature difference between slab and interior at mid-depth, increases with aspect ratio (Fig. 7), which indicates that long wavelength flows are driven by larger buoyancy forces than short wavelength flows.

4.5 Transition from Poiseuille flow to Couette flow in asthenosphere

From Fig. 4 we expect many of our simulations to fall into a transition regime between end-member Poiseuille and Couette flow types. We hypothesize that the transition between Poiseuille flow (sluggish lid) and Couette flow (active lid) is associated with the increase in available buoyancy at large wavelengths.

Poiseuille flows are characterized by strongly channelized flow in the low-viscosity channel and negligible plate velocities. We predict that buoyancy forces at work in this regime cannot overcome the resistance to motion associated with the near-surface plate, the effective bending resistance, which results in sluggish lid convection. Our hypothesis is motivated by Solomatov (1995), who used a

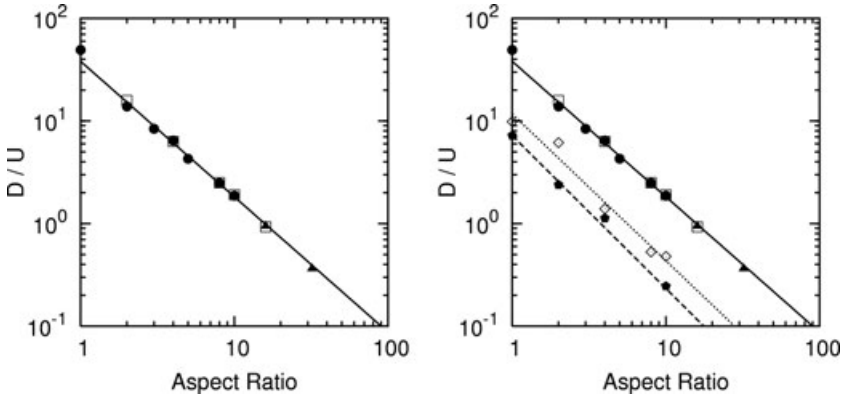

Figure 8. D/U versus aspect ratio. (a) A universal power law relation is found for all simulations with a lithosphere/asthenosphere viscosity ratio of 1000. The equation that best fits the data is $D/U = (38.2 \pm 1.0)\ \Gamma^{-1.328\pm0.018}$. (b) Additional simulations with a 10-times lower viscosity ratio $\mu_L/\mu_A = 100$ show transitions between Poiseuille flow and Couette flow in the asthenosphere ($D/U \approx 1$) at smaller aspect ratios . Best fits are $D/U = (7.2 \pm 1.1)\ \Gamma^{-1.44\pm0.08}$ (closed symbols, weaker plate) and $D/U = (11.7 \pm 1.2)\ \Gamma^{-1.43\pm0.13}$ (open symbols, stronger low-viscosity channel).

scaling analysis of temperature- and stress-dependent viscosity convection to predict three different regimes: (1) an active lid regime (small viscosity contrast regime), in which plates move faster than the interior; (2) a sluggish regime (transitional regime), in which plates move slower than internal flow and (3) a stagnant lid regime with zero plate velocity. The sluggish regime is characterized by the self-controlled dynamics of the cold boundary layer and occurs when plate-bending resistance is comparable to viscous drag in the interior (Solomatov 1995). Altough Solomatov (1995) did not consider an asthenosphere or wavelength effects, his general ideas still serve as a guide to us. We note that Tackley (2000) observed models with an active lid to develop the longest possible wavelength.

In contrast to Poiseuille flow, Couette flow shows the largest velocities at the plates and occurs when active plate-bending becomes relatively weak. We conjecture that this happens when buoyancy forces at work in this regime overcome the effective bending resistance of plates at converging margins, resulting in active, or mobile lid convection.

The transition between Poiseuille flow regime and Couette flow regime should therefore be connected to quantities derived from energetics, the resistance to motion associated with both the near-surface plate and the low-viscosity channel. Before we focus on this aspect, we will consider an important variable in the characterization between Poiseuille and Couette flows.

In the previous section, it has become clear that both the Poiseuille component D and the Couette component U of the velocity in the low-viscosity channel depend on the length of the convection cell, the aspect ratio Γ. The variable D/U characterizes the flow type in the low-viscosity channel, indicating its importance for this system. In order for this ratio to be relatively large, the effective bending resistance must be large relative to the resistance that comes from the low-viscosity asthenosphere. An interesting and surprising result is that D/U depends on the aspect ratio Γ in form of a universal power law. Fig. 8(a) shows this relation (Fig. 8b will be discussed later). The best fit through the data is given by

$$D/U = (38.2 \pm 1.0)\Gamma^{-1.328\pm0.018}. \quad (5)$$

The fact that this relation is valid for both regimes allows us to predict the aspect ratio at which the transition between Poiseuille flow to Couette flow occurs. An expectation is that the transitions in scaling behaviour observed in our numerical outputs (Fig. 2) will initiate once the Poiseuille and Couette components become

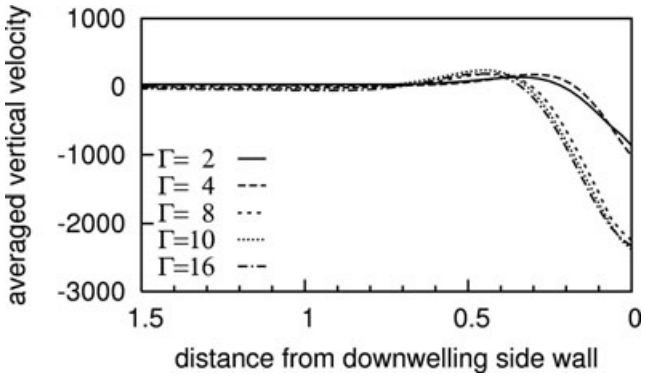

Figure 9. Averaged vertical velocity curves fall into two families depending on aspect ratio. The extent from the wall to the velocity maximum indicates the shear scale associated with the slab. Small aspect ratio simulations show a smaller shear scale than large aspect ratio simulations.

comparable as this would indicate that plate-bending resistance is no longer a significant viscous work term in the system energy balance. Substituting $D/U = 1$ into eq. (5) and solving for Γ predicts a transition aspect ratio of $\Gamma_{tr} \approx 16$. This estimate is not in precise agreement with numerical outputs (Fig. 2) but it is reasonable if we consider that the flow components will become comparable slightly before the D/U ratio hits unity.

The transition in scaling regimes observed for near-surface quantities should also occur for internal quantities. Once the effective bending resistance of the plate becomes low, the scaling for the descending plate velocity should change and an expectation is that the vertical shear in the bulk mantle would be effected. Fig. 9 shows the averaged vertical velocities from simulations in the small 3-D geometry with different aspect ratios. Two families of curves can be identified, one for small aspect ratios and one for large aspect ratios ($\Gamma \geq 8$). The scale of shear due to slab descent is ≈0.3 for small aspect ratios and ≈0.45 for large aspect ratio simulations.

If our interpretation for the regime transitions is correct, then specific predictions should hold. Lowering the relative viscosity of the surface plate should cause the transition to occur at smaller aspect ratios as the effective bending resistance will be lower. This should also hold for a larger resistance to motion in the asthenosphere, which can be simulated by increasing the relative viscosity in the

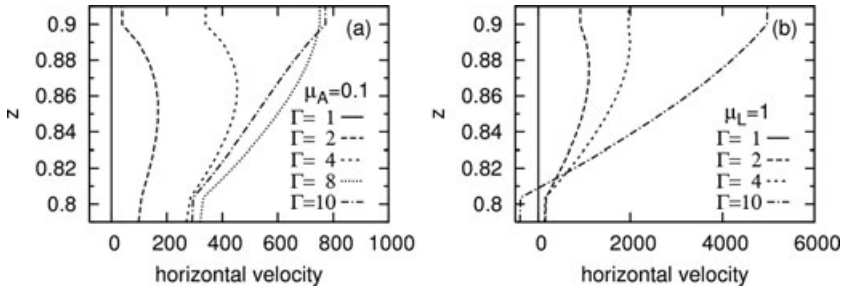

Figure 10. Velocity profiles in the low-viscosity channel for simulations with a lithosphere/asthenosphere viscosity ratio of 100. (a) $\mu_L = 10$, $\mu_A = 0.1$ and (b) $\mu_L = 1$, $\mu_A = 0.01$. Both sets of simulations show a transition between Poiseuille flow and Couette flow at an aspect ratio between 4 and 10, which is a shift to smaller aspect ratios with respect to simulations with a lithosphere/asthenosphere viscosity ratio of 1000.

low-viscosity channel. We performed additional simulations to test these predictions.

4.6 Relative viscosity between lithosphere and asthenosphere

If the transition between Poiseuille flow and Couette flow in the asthenosphere is connected to the relative resistance to motion of the near-surface plate to the relative resistance to motion in the low-viscosity channel, then one would expect the transition to occur at smaller wavelengths for both, a weaker near-surface zone and a stronger low-viscosity channel. To test these predictions, we performed two additional suites of simulations with different aspect ratios ranging from 1 to 10, for which we changed the viscosity ratio of near-surface plate to low-viscosity channel by one order of magnitude to $\mu_L/\mu_A = 100$. For the first suite we lowered the near-surface viscosity to $\mu_L = 1$ ($\mu_A = 0.01$) and for the second suite we increased the viscosity in the low-viscosity channel to $\mu_A = 0.1$ ($\mu_L = 10$) while keeping everything else the same.

In Fig. 10, we show the velocity profiles in the low-viscosity channel as a function of aspect ratio for both suites of simulations with a reduced viscosity ratio. Both suites of simulations show a transition between Poiseuille flow and Couette flow at an aspect ratio smaller than that for simulations with a larger lithosphere/asthenosphere viscosity ratio.

For statistically steady states in both suites we observe Poiseuille–Couette flow in the asthenosphere and the Poiseuille–Couette magnitude ratio D/U to decrease with aspect ratio as shown in Fig. 8(b). For both additional suites, we find that D/U approaches 1 for smaller aspect ratios than in the previous simulations with a larger viscosity contrast between lithosphere and asthenosphere. Interestingly, the exponent in the $D/U - \Gamma$ relation is in good agreement with previous simulations, which indicates that it is independent of the relative plate and asthenosphere viscosities.

The transition between Poiseuille flow and Couette flow in the asthenosphere, and correspondingly between sluggish and active plates, is connected to a criteria based on the energetics of the system that is associated with the relative resistances to motion from plate-bending and flow in the asthenosphere. This result was obtained from simulations with a prescribed vertically layered viscosity structure that simulates a weak asthenosphere below a compositionally stronger boundary layer. We will now corroborate our findings with simulations in which a high-viscosity upper boundary layer underneath a low-viscosity layer is generated by a viscoplastic rheology.

4.7 Viscoplastic models

We chose a temperature- and depth-dependent viscoplastic rheology that allows for the dynamic formation of a high-viscosity upper boundary layer and a submerged low-viscosity channel, analogs for plates and the asthenosphere, respectively. The viscoplastic rheology employed (Moresi & Solomatov 1998) permits weak zones to form in regions where a critical yield stress is reached. These zones are model analogs for plate boundaries. They allow the otherwise cold, and hence high viscosity, upper boundary layer to partake in convective overturn and cool the interior mantle.

For stresses below a specified yield, τ_y, the rheology law follows a temperature-dependent viscous branch given by

$$\mu_{\text{creep}} = A_{(u,l)} \exp[-\theta_{(u,l)} T], \tag{6}$$

where $A_{(u,l)}$ and $\theta_{(u,l)}$ are material parameters that can be set to different values for the upper (u) and lower (l) mantle to facilitate the dynamic generation of plate analog and asthenosphere analog, T is temperature and μ is mantle viscosity. A reference viscosity, μ_0, is defined from eq. (6) at the mantle's surface temperature. Stress is non-dimensionalized by $d^2/\kappa\mu_0$, where d is the mantle depth and κ is the mantle thermal diffusivity. The non-dimensional yield stress is defined as:

$$\tau_y = \tau_{y0} + \tau_{yz} z, \tag{7}$$

where τ_{y0} is a surface value, τ_{yz} is a depth-dependent term, and z is a non-dimensional depth coordinate. The τ_{yz} term is non-dimensionalized by $(f_c \text{Ra}_0)/(\alpha \Delta T)$, where f_c is a friction coefficient, Ra_0 is the mantle Rayleigh number defined using the reference viscosity, and ΔT is the temperature drop across the mantle. At the yield stress, the flow law switches to a plastic branch with an effective viscosity given by

$$\mu_{\text{plastic}} = \tau_y / I, \tag{8}$$

where I is the second strain-rate invariant. This formulation allows localized zones of lithospheric failure, analogs to plate boundaries, to form in a self-consistent manner. The failure zones allow for the potential of lithospheric recycling akin to plate tectonics on present day Earth.

We present the results from two simulations suites that represent relative weak and relatively strong plate boundaries. The lithospheric yield stress was varied by changing the non-dimensional surface value, τ_{y0}, while holding the depth-dependent term fixed at a non-dimensional value of 3.0. For the weak boundaries suite $\tau_{y0} = 3.0$ and for the strong suite $\tau_{y0} = 7.0$. For both suites $\text{Ra}_0 = 100$ and the internal to basal heating Rayleigh number ratio is

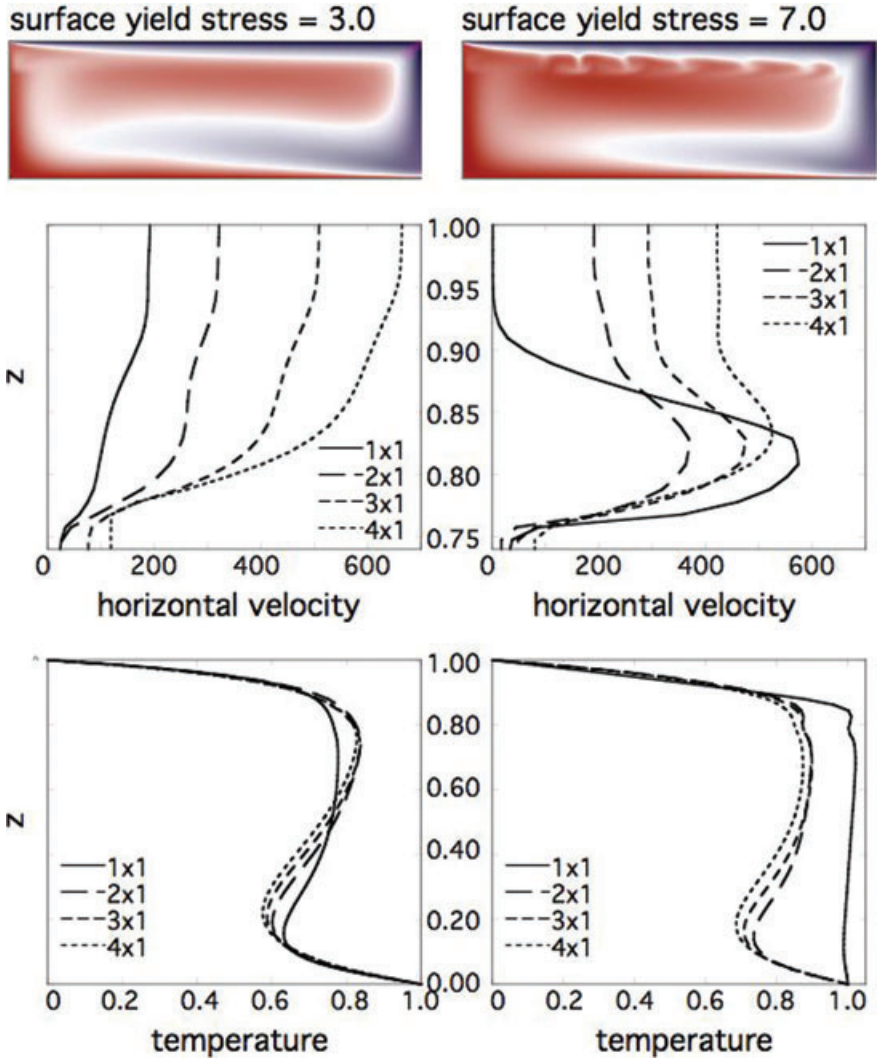

Figure 11. Results from simulations with viscoplastic rheology. Different surface yield stresses have been used, $\sigma_{y0} = 3.0$ (left panels) and $\sigma_{y0} = 7.0$ (right panels). (a, b) Temperature snapshots of statistically steady state for aspect ratio 4. (c, d) Horizontal velocity profiles in low-viscosity channel and high-viscous upper boundary layer for different aspect ratios. (e, f) Horizontally averaged temperature profiles for different aspect ratios.

two. For the suites presented, a viscosity jump from the upper to the lower mantle was modelled by changing the value of the activation temperature, θ at a non-dimensional depth of 0.25 (added modelling suites showed that our main qualitative conclusions are robust for cases in which θ is fixed with depth but the pre-exponential term, A, in the viscosity law is varied with depth). The value of θ for the upper mantle allows for a six order of magnitude viscosity reduction from the surface to the base mantle temperature. The value of θ for the lower mantle allows for a three order of magnitude viscosity reduction from the surface to the base mantle temperature. This formulation allows the upper boundary layer to have a high viscosity to mimic a plate. The exponential decrease of viscosity with temperature allows the mantle below the plate analog to be weak and together with the viscosity increase at a depth of 0.25, due to different activation temperatures, the formulation also allows for the generation of a low-viscosity channel.

Results from these simulations are summarized in Fig. 11. For both suites, we observe Poiseuille–Couette flow in the low-viscosity channel. For a relatively high yield strength, an analog to strong plate boundaries, we find a strong Poiseuille component and an increasing plate velocity with aspect ratio, which leads to an increasing Couette component. The relatively high yield strength cases are comparable to the Poiseuille flow regime we have observed at short wavelengths. In contrast, for a relatively low yield strength, an analog for weak plate boundaries, we find a dominating Couette flow component in the low-viscosity channel, which is comparable to the long wavelength regime. We conclude that the resistance to motion in the upper boundary layer is connected to its yield strength, a region that in the context of plate tectonics translates to the plate boundary. This in turn suggests that the strength of plate boundaries has a direct influence on the solid-state mantle flow within the asthenosphere as characterized by the Poiseuille/Couette magnitude ratio D/U.

We find that for the weak boundary suite 64 per cent (1×1 cell) to 62 per cent (4×1 cell) of the surface heat flow come from internal heating; for the strong boundary suite this ratio is between 99 per cent (1×1 cell) and 68 per cent (4×1 cell), all consistent with our findings that large aspect ratio convection (active lid) allows for more efficient heat transport across the mantle than short aspect ratio (sluggish lid).

Our viscoplastic simulations and layered -viscosity simulations alike show that both, a sluggish lid convection mode and an active lid convection mode, can exist for the same level of convective vigour (e.g. Rayleigh number) but at different convective wavelengths.

5 IMPLICATIONS FOR CONVECTION ON EARTH

Based on kinematic and energetic criteria, we have mapped two regimes that suggest a connection between solid-state flow in the asthenosphere and the relative strength of plate boundaries. We find that Poiseuille flow in the asthenosphere is connected to relatively strong plate margins and sluggish or slowly moving plates. In this regime, a significant resistance to motion is due to plate-bending. The other regime shows Couette flow in the asthenosphere and is connected to relatively weak plate margins and active lid convection. Viscous shear in the bulk mantle that is associated with the downwelling slab provides most resistance to motion.

Different observations may potentially be able to discriminate between Poiseuille and Couette regimes in Earth's mantle. For example, a lateral pressure gradient in the asthenosphere may produce a signal in topography, and lead to predictions that can be tested by an analysis of seafloor bathymetry. Vertical flow associated with small-scale convection underneath old lithosphere may complicate topography signals at wavelengths comparable to the size of small-scale convection rolls. However, this complication is not expected for younger lithosphere, for which our simulations predict a distinct difference between Poiseuille flow and Couette flow. Although this study is not focussed on this aspect, our simulations indicate that Poiseuille flow is associated with a larger surface topography gradient and larger surface heatflux gradient over the entire convection cell.

Other observations involve strain rate distribution in the asthenosphere and in turn the development of seismic anisotropy. Continued measurement of the radial anisotropic shear velocity structure (e.g. Nettles & Dziewoński 2008) with increased vertical resolution may allow to discriminate between Poiseuille and Couette flow regimes. Couette flow is associated with a near uniform velocity gradient in the asthenosphere, whereas Poiseuille flow has a relatively low-velocity gradient in the centre of the asthenosphere and two peaks near the top and base of the asthenosphere. This difference should correlate with a different anisotropy signals in the asthenosphere. In particular, a uniform anisotropy pattern within the asthenosphere would favour the Couette regime. As the two regimes, Couette versus Poiseuille, depend on the relative strength of plate margins, this suggests that seismic observations focussed on the asthenosphere could provide an indirect constraint of the relative strength of plate margins.

The interaction between the asthenosphere and plates leads to an implication regarding the mode of mantle convection and the Earth's thermal history. In recent thermal history models, a sluggish lid regime of mantle convection has been invoked to reconcile thermal history predictions with observations related to the Earth's thermal state, in particular the mantle Urey ratio (Conrad & Hager 1999; Korenaga 2003). The original work on the sluggish lid regime (transitional regime) by Solomatov (1995) found it to be viable over a highly limited parameter regime. This would make invoking the regime over the history of the Earth, within thermal history studies, a tenuous exercise. Allowing for plate margin failure does not alleviate this problem. Numerical simulations employing viscoplastic rheologies to mimic plate margin failure show a rapid transition between active and stagnant lid convection (e.g. Moresi & Solomatov 1998). This indicates that allowing for plate-like behaviour does not, on its own, extend the robustness of the sluggish lid regime. The work noted above did not consider the interaction between the asthenosphere and plates. Our work indicates that these interactions open up the possibility that the sluggish lid mode is more robust than previously thought. Further, our work shows that the transition between a sluggish and an active lid regime is wavelength dependent. This opens the possibility that plate tectonics may operate in a combination of active and sluggish lid convection, both in time due to changes in convective wavelength and potentially in space due to variations in plate dimensions.

6 CONCLUSIONS

We demonstrate that mixed heated 3-D mantle convection simulations with a low-viscosity asthenosphere submerged underneath a high-viscosity lithosphere leads to very long convection cells. We find a relatively short and a long wavelength regime in which surface velocity and surface heat flux scale differently with cell length. The regime transition is characterized by a maximum heat flux.

Our simulations show that mantle flow in the lithosphere–asthenosphere region is a Poiseuille–Couette flow. The Poiseuille component dominates in the short wavelength regime where velocity amplitudes in the asthenosphere exceed surface velocities. The lateral pressure gradient driving Poiseuille flow in the asthenosphere is associated with low pressure regions generated near subduction zones.

As the wavelength of convection increases, we find a distinct break in the scaling behaviour of heat flux versus cell length, and surface velocities exceed asthenosphere velocity. Flow in the asthenosphere becomes dominated by the Couette component. The internal temperature is correlated with heat flux and changes as a function of aspect ratio.

The Poiseuille/Couette velocity magnitude ratio, D/U, allows to characterize solid-state flow in the asthenosphere and to predict the regime transition. The transition depends on the relative strength of lithosphere and asthenosphere and is associated with a switch in the dominant resistance to convective motion. In the Poiseuille regime, plate-bending provides a significant resistance force, whereas in the Couette regime, the dominant resisting force comes from vertical shear in the bulk mantle.

The Couette regime agrees with classical scaling ideas for mantle convection, whereas the Poiseuille regime is an example of a sluggish lid mode of mantle convection which has been the focus of more recent thermal history models of the Earth. Our simulations show that both modes can exist for the same level of convective vigour (i.e. Rayleigh number) but at different convective wavelengths.

Additional simulations with temperature- and yield-stress-dependent viscosity show consistent behaviour and further suggest that the regime crossover is also associated with the relative strength of plate margins. Short wavelength cells are associated with relatively low negative buoyancy in subducting slabs that allows the resistance to plate-bending to slow surface velocities. The negative buoyancy increases with cell wavelength and at the regime transition it overcomes the bending resistance. Our simulations establish a connection between the strength of plate margins, solid-state flow in the asthenosphere, and the wavelength of mantle convection. This connection suggest that plate tectonics in the sluggish lid mode is wavelength dependent and is potentially more robust than previously envisioned.

ACKNOWLEDGMENTS

Authors thank Mark Richards for many discussions. Authors acknowledge Shijie Zhong and an anonymous reviewer for constructive comments. This research was supported by NSF and in parts by the Rice Computational Cluster funded by NSF under grant CNS-0421109, by the Shared University Grid at Rice funded by NSF under Grant EIA-0216467, by a partnership between Rice University, AMD and Cray and by a partnership between Rice University, Sun Microsystems, and Sigma Solutions, Inc.

REFERENCES

Anderson, D.L. & Sammis, C., 1970. Partial melting in the upper mantle, *Phys. Earth planet. Inter.,* **3,** 41–50, doi:10.1016/0031-9201(70)90042-7.

Anderson, D.L. & Spetzler, H., 1970. Partial melting and the low-velocity zone, *Phys. Earth planet. Inter.,* **4**(1), 62–64.

Bunge, H.-P., Richards, M.A. & Baumgardner, J.R., 1996. Effect of depth-dependent viscosity on the planform of mantle convection, *Nature* **379**(6564), 436–438, doi:10.1038/379436a0.

Bunge, H.-P., Richards, M.A. & Baumgardner, J.R., 1997. A sensitivity study of three-dimensional spherical mantle convection at 10^8 Rayleigh number: effects of depth-dependent viscosity, heating mode, and an endothermic phase change, *J. geophys. Res.,* **102,** 11 991–12 008, doi:10.1029/96JB03806.

Busse, F.H., Richards, M.A. & Lenardic, A., 2006. A simple model of high Prandtl and high Rayleigh number convection bounded by thin low-viscosity layers, *Geophys. J. Int.,* **164**(1), 160–167, doi:10.1111/j.1365-246X.2005.02836.x.

Conrad, C.P. & Hager, B.H., 1999. The thermal evolution of an Earth with strong subduction zones, *Geophys. Res. Lett.,* **26**(19), 3041–3044.

Gutenberg, B., 1959. *Physics of the Earth's Interior*, Academic Press, New York.

Hager, B.H. & Richards, M.A., 07 1989. Long-wavelength variations in Earth's geoid: physical models and dynamical implications. *Phil. Trans. R. Soc. Lond. A, Math. Phys. Sci. (1934–1990),* **328**(1599), 309–327.

Harder, H., 2000. Mantle convection and the dynamic geoid of Mars, *Geophys. Res. Lett.,* **27,** 301–304.

Hirth, G. & Kohlstedt, D.L., 1996. Water in the oceanic upper mantle: implications for rheology, melt extraction and the evolution of the lithosphere, *Earth planet. Sci. Lett.,* **144**(1–2), 93–108.

Höink, T. & Lenardic, A., 2008. Three-dimensional mantle convection simulations with a low-viscosity asthenosphere and the relationship between heat flow and the horizontal length scale of convection, *Geophys. Res. Lett.,* **35**(L10304), doi:10.1029/2008GL033854.

Karato, S.-i. & Jung, H., 1998. Water, partial melting and the origin of the seismic low velocity and high attenuation zone in the upper mantle, *Earth planet. Sci. Lett.,* **157**(3-4), 193–207.

Korenaga, J., 2003. Energetics of mantle convection and the fate of fossil heat, *Geophys. Res. Lett.,* **30**(8), 080000–1, doi:10.1029/2003GL016982.

Lenardic, A., Richards, M.A. & Busse, F.H., 2006. Depth-dependent rheology and the horizontal length scale of mantle convection, *J. geophys. Res.,* **111,** B07404, doi:10.1029/2005JB003639.

Marone, F. & Romanowicz, B., 2007. The depth distribution of azimuthal anisotropy in the continental upper mantle, *Nature,* **447**(7141), 198–201.

McNamara, A.K. & Zhong, S., 2005. Degree-one mantle convection: dependence on internal heating and temperature-dependent rheology, *Geophys. Res. Lett.*, **32,** L01301, doi:10.1029/2004GL021082.

Moresi, L. & Gurnis, M., 1995. Constraints on the lateral strength of slabs from three-dimensional dynamic flow models, *Earth planet. Sci. Lett.,* **138,** 15–28, doi:10.1016/0012-821X(95)00221-W.

Moresi, L. & Solomatov, V.S., 1998. Mantle convection with a brittle lithosphere: thoughts on the global tectonic styles of the Earth and Venus, *Geophys. J. Int.,* **133**(3), 669–682, doi:10.1046/j.1365-246X.1998.00521.x.

Morgan, J.P., Morgan, W.J., Zhang, Y.-S. & Smith, W.H.F., 1995. Observational hints for a plume-fed, suboceanic asthenosphere and its role in mantle convection, *J. geophys. Res.,* **100,** 12 753–12 768, doi:10.1029/95JB00041.

Morgan, J.P. & Smith, W.H.F., 1992. Flattening of the sea-floor depth-age curve as a response to asthenospheric flow, *Nature,* **359**(6395), 524–527.

Nettles, M. & Dziewoński, A.M., 2008. Radially anisotropic shear velocity structure of the upper mantle globally and beneath North America, *J. geophys. Res.* **113,** B02303, doi:10.1029/2006JB004819.

Paulson, A. & Richards, M.A., 2009. On the resolution of radial viscosity structure in modeling long-wavelength post-glacial rebound data, *Geophys. J. Int.,* in press, doi:10.1111/j.1365-246X.2009.04362x.

Richards, M.A., Yang, W.-S., Baumgardner, J.R. & Bunge, H.-P., 2001. Role of a low-viscosity zone in stabilizing plate tectonics: implications for comparative terrestrial planetology', *Geochem. Geophys. Geosyst.,* **2** (2000GC000115), doi:10.1029/2000GC000115, 2001.

Roberts, J.H. & Zhong, S., 2006. Degree-1 convection in the Martian mantle and the origin of the hemispheric dichotomy, *J. geophys. Res.,* **111**(E10), E06013, doi:10.1029/2005JE002668.

Solomatov, V., 1995. Scaling of temperature- and stress-dependent viscosity convection, *Phys. Fluids,* **7**(2), 266–274.

Stixrude, L. & Lithgow-Bertelloni, C., 2005. Mineralogy and elasticity of the oceanic upper mantle: origin of the low-velocity zone, *J. geophys. Res.,* **110**(B9), B03204, doi:10.1029/2004JB002965.

Su, W.-J. & Dziewonski, A.M., 1992. On the scale of mantle heterogeneity, *Phys. Earth planet. Int.,* **74**(1-2), 29–54.

Tackley, P.J., 1996. On the ability of phase transitions and viscosity layering to induce long wavelength heterogeneity in the mantle, *Geophys. Res. Lett.,* **23,** 1985–1988, doi:10.1029/96GL01980.

Tackley, P.J., 2000. Self-consistent generation of tectonic plates in time-dependent, three-dimensional mantle convection simulations, 1, Pseudoplastic yielding, *Geochem. Geophys. Geosyst.,* **1**(8), 1021, doi:10.1029/2000GC000036.

Thoraval, C. & Richards, M.A., 1997. The geoid constraint in global geodynamics: viscosity structure, mantle heterogeneity models and boundary conditions, *Geophys. J. Int.,* **131,** 1–8.

Yamamoto, M., Morgan, J.P. & Morgan, W.J., 2007. Global plume-fed asthenosphere flow i: motivation and model development. Special Paper 430: *Plates, Plumes planet. Proc.,* **430**(0), 165–188, doi:10.1130/2007.2430(09).

Zhong, S., 2006. Constraints on thermochemical convection of the mantle from plume heat flux, plume excess temperature, and upper mantle temperature, *J. geophys. Res.,* **111** (B04409), doi:10.1029/2005JB003972.

Zhong, S., Zhang, N., Li, Z.-X. & Roberts, J.H., 2007. Supercontinent cycles, true polar wander, and very long-wavelength mantle convection, *Earth planet. Sci. Lett.,* **261**(3–4), 551–564.

Zhong, S., Zuber, M.T., 2001. Degree-1 mantle convection and the crustal dichotomy on Mars, *Earth planet. Sci. Lett.,* **189,** 75–84(10), doi:10.1016/S0012-821X(01)00345-4.